

Five-Level Common-Ground Inverter Topology Using an Integrated Charge-Pump and Switched-Capacitor Network

Anup Marahatta, *Student Member, IEEE*, Shafiuzzaman Khadem, *Senior Member, IEEE* and Sandipan Patra, *Senior Member, IEEE*

Abstract— This paper presents a novel five-level common-ground (CG) inverter topology designed for transformerless residential photovoltaic (PV) applications. The proposed inverter integrates a switched-capacitor (SC) network with a charge-pump mechanism, enabling continuous capacitor charging during both positive and negative half-cycles of the grid voltage. This innovation addresses the long-standing issue of capacitor voltage decay in CG multilevel inverters, thereby reducing the required DC-link capacitance while maintaining voltage stability under high-power operation. The topology inherently balances capacitor voltages through alternating series-parallel switching, eliminating the need for additional sensing or active control circuits. Compared with conventional CG designs, the proposed inverter achieves higher power density and reduced capacitance requirements, while preserving low leakage current, minimised dv/dt stress, and reduced electromagnetic interference (EMI). A comprehensive evaluation is conducted through hardware-in-the-loop (HIL) simulations in both standalone and grid-connected modes. Results demonstrate that the inverter achieves 96.4% efficiency at a 7 kW rating with capacitor requirements reduced by more than 70% compared with state-of-the-art topologies with a similar no of switches. These findings establish the proposed topology as a compact, efficient, and reliable solution for next-generation residential PV grid integration.

Index Terms—Common-ground inverter; Five-level inverter; Switched-capacitor; Charge-pump; Capacitor voltage balancing; Transformerless PV inverter; Grid integration; HIL Simulation.

I. INTRODUCTION

Residential solar photovoltaic (PV) systems are increasingly deployed, turning consumers into “prosumers” who not only draw energy from the grid but also feed surplus solar power back into it. Grid-connected inverters are the key enabling technology for these systems, converting DC power from PV panels into grid-compliant AC and ensuring the injected current meets stringent grid codes for safety, power quality, and stability [1]. Modern inverters do more than simple DC–AC conversion; they often support ancillary services such as power factor correction, reactive power support, and voltage regulation [2]. In this context, multilevel inverter topologies have gained popularity for grid-tied applications due to their superior output power quality, reduced switching stress, and higher efficiency compared to traditional two-level designs [3]. By synthesising the AC waveform from multiple smaller voltage steps, multilevel inverters achieve lower total harmonic distortion (THD) and allow the use of smaller output filters. They also distribute voltage stress across components, potentially improving reliability and extending the lifespan of components [4].

In recent years, transformerless inverters have gained popularity for small and medium-scale PV installations due to their higher efficiency, lower cost, reduced size, and improved power density (achieved by eliminating the bulky line-frequency transformer). For transformerless PV inverters, an important consideration is the suppression of leakage currents caused by the PV array’s parasitic capacitance to ground [5]. High-frequency switching of the inverter can induce common-mode voltage fluctuations, which in turn drive a current through the parasitic capacitance between the PV panels and ground [6]. This undesirable common-mode current (leakage current) can pose safety hazards and lead to energy losses of a few per cent in efficiency if not mitigated [7]. A common solution is to use common-ground inverter configurations, in which the negative terminal of the PV array is directly connected to the neutral of the grid (ground), eliminating large common-mode voltage swings [6],[7]. Such common-ground or “zero common-mode” topologies inherently keep the PV array referenced to ground at all times, greatly reducing leakage currents, which amount up to 3% efficiency [5]. Combining the multilevel approach with a common-ground configuration is therefore highly attractive for PV systems, as it promises both high power quality and minimal ground leakage current [8].

Recent research in multilevel inverters for PV has focused on improving efficiency and power density while reducing complexity and cost [9]. Many new topologies aim to minimise the number of power electronic components (switches, diodes, capacitors) and to simplify control, all while delivering the benefits of multilevel waveforms. In the specific domain of five-level inverters suitable for single-phase PV, a number of transformerless (galvanically isolated only through the DC link) designs have been proposed [10]. A critical challenge identified in these common-ground multilevel architectures is the need to maintain stable intermediate voltage levels (e.g., the mid-point or flying capacitor voltages) throughout the AC grid cycle. Because the PV negative is tied to ground, certain conventional charging paths for flying or split capacitors are blocked during portions of the waveform (specifically, during the generation of negative output voltage levels). As a result, existing common-ground multilevel inverters often rely on large DC-link or flying capacitors to hold charge when the circuit cannot refresh them every cycle [9], [11]. Oversized capacitors

can reduce the voltage droop during those intervals, but they run counter to the goal of high power density and add cost. There is thus a design trade-off between maintaining voltage balance (via large capacitances or complex control) and keeping the inverter compact, which can be observed in [12],[13]. Authors in [12] introduced a five-level common-ground inverter that produces excellent output quality and eliminates ground leakage; however, it requires a relatively large DC-link capacitor and its flying capacitor experiences voltage decay during the negative half-cycle of the grid voltage. This results in a restricted power output range unless the capacitor is significantly oversized, as the capacitor cannot be recharged at certain output levels. Similar difficulties with capacitor voltage imbalance and limited charging opportunities are observed in other recent common-ground multilevel topologies [12], [13], [14], [15], [16], [17]. These limitations indicate a clear gap in the state-of-the-art: no existing five-level common-ground design simultaneously achieves small passive components, balanced capacitor voltages, and high-power performance without resorting to complex control and capacitor oversizing.

To address this gap, this paper proposes a novel five-level common-ground inverter topology that uses an integrated switched-capacitor network with a charge-pump mechanism to maintain capacitor voltages throughout the AC cycle. The design is inspired by two key concepts from recent literature. First is the integration of a flying capacitor within the H-bridge leg, as demonstrated in a three-level inverter in [18]. By inserting a floating capacitor and appropriate switching arrangements into a single-phase H-bridge, this approach created a high-power three-level common ground topology. Second, the use of a charge-pump or switched-capacitor assistance circuit, as employed in [11] in a three-level topology, to actively transfer charge and keep the intermediate capacitor voltage balanced during both halves of the grid cycle. Building on these ideas, the proposed topology replaces the single flying capacitor of a [18] with a switched-capacitor cell that can be reconfigured to either series or parallel mode. Unlike prior common-ground multilevel designs, which could only charge their flying capacitors during the positive half-cycle or zero-voltage states [12], the proposed new topology uses a charge-pump circuit to also recharge the capacitors during the negative half-cycle. This effectively eliminates the problem of capacitor voltage sag/decay at the negative peak ($-2V$ level) of the output. As a result, the required capacitance value is significantly reduced. The proposed design can maintain a stable voltage with much smaller capacitors. This enables the inverter to supply higher power with smaller capacitors, thereby improving power density without sacrificing performance. The concept leverages the common-ground H-bridge structure of [18], the capacitor charging method of [11] and the multilevel generation method of [12] to develop a new common ground multilevel topology.

The proposed five-level inverter topology offers several notable advantages over the existing state-of-the-art. Such as;

- First, by continuously charging the DC-link and flying capacitors through the charge pump action, it significantly reduces the size of the DC-link capacitor and any flying capacitors without incurring voltage imbalance, thereby raising the achievable power capacity of the system.
- Second, the five-level output waveform inherently has a lower step voltage (approximately one-half of the DC link voltage per step, in this design), which leads to a lower dv/dt at each switching transition. In combination with the common-ground configuration, this means the inverter exhibits negligible leakage current, reduced electromagnetic interference (EMI), and allows the use of a smaller output filter while still meeting harmonic standards as per [19].
- Third, the switched-capacitor network in the topology is self-balancing: the way the capacitors are connected and charged in alternating patterns ensures their voltages naturally equalise, eliminating the need for complex voltage sensing or active balancing control circuits.
- Finally, the topology maintains high conversion efficiency by avoiding energy losses associated with leakage currents and by operating the switches at optimal states (each device sees lower stress and can switch at a lower frequency compared to an equivalent two-level inverter for the same performance).

Overall, the proposed inverter achieves a compelling combination of improved harmonic performance, high efficiency, and enhanced power capacity in a transformerless, common-ground configuration ideally suited for residential PV installations.

The remainder of this paper is structured as follows: Section II provides a detailed introduction of the proposed five-level inverter topology, explaining its circuit configuration, operating principle, and how the charge-pump-based switched-capacitor network functions over a grid cycle. Design considerations, including component selection and flying capacitor sizing, are also discussed. Section III demonstrates the validation of the topology and the control strategy in a hardware-in-the-loop (HIL) real-time synchronisation environment. Section IV discusses the test conditions and experimental results, demonstrating the performance improvements (in terms of leakage current, THD, efficiency, etc.) of the proposed inverter against conventional designs. Finally, Section V concludes the paper by summarising the key contributions and suggesting directions for future work.

II. PROPOSED TOPOLOGY

Fig. 1 shows the proposed five-level common ground topology. It consists of a series/parallel switched capacitor circuit placed inside an H-Bridge to generate a five-level output voltage. It also has a charge pump circuit to charge the switched capacitor cell during the negative half cycle, ensuring a stable voltage across the capacitors at all times. The topology has ten switches and requires eight gate drivers.

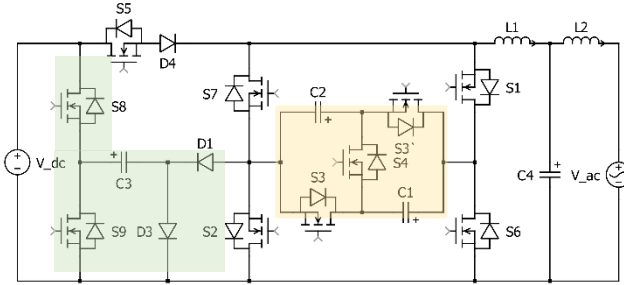


Fig. 1. Proposed five-level topology

The main advantage of the proposed topology is the reduction of the size of the floating capacitors. The switched capacitor cell is charged directly from the source during the positive half cycle, and it is charged through a charge pump circuit during the negative half cycle. This configuration enables the reduced capacitor size and the circuit to function on a common ground configuration at high power output conditions. The switched capacitor cell delivers the power at all voltage levels. The same switched capacitor cell can also absorb the reactive power at all voltage levels, allowing the inverter to generate distortion-free five-level output even in reactive power compensation mode.

Existing common ground five-level inverter topologies have the issue of excessive capacitor voltage decline during the negative operating cycle. This occurs as the topologies cannot charge the flying capacitors at a certain output voltage level during the generation period. Due to this, the output waveform is distorted at higher power levels. The proposed topology uses charge pump circuits to maintain the capacitor voltage at levels at all operating conditions. The voltage fluctuation across the capacitors is given by the following equations:

$$\Delta V_{1,2} = \frac{1}{C_{1,2}} \left(\int_{T-t_{ser}}^T \frac{i_o(t)}{2} dt - \int_{T-t_{parr}}^T \frac{i_{pump}(t)}{2} dt \right) \quad (1)$$

Where T is the switching period and t_{ser} is time spent under a serial connection and t_{parr} is the time under parallel mode in each switching period and $i_o(t)$ is the output current and $i_{pump}(t)$ is the charging current for parallel and series mode, respectively. To maintain a stable voltage across the flying capacitors, the power pumped by the charge pump capacitor should be equal to the instantaneous power being output by the inverter.

Let the peak output power begin to be delivered by the inverter be P_{out} and the voltage level we aim to maintain in the capacitors be V_{dc} and peak output current be I_{out} . To maintain the capacitor voltage within the limit, the net charge in the capacitor should also change within a certain limit. The charge fluctuation and minimum capacitance required for the series parallel cell are given by the following equations:

$$I_{out} = \frac{P_{out}}{V_{dc}} \quad (2)$$

$$\Delta Q_{C1,C2} = I_{out} \cdot T_{discharge} = \frac{P_{out}}{V_{dc}} M_{index} * T \quad (3)$$

$$C_{1,2} \Delta V = \frac{P_{out}}{V_{dc}} M_{index} * T \quad (4)$$

$$C_{1,2} = \frac{P_{out} M_{index}}{V_{dc} f_{sw} \Delta V} \quad (5)$$

The proposed inverter synthesises five discrete voltage levels by operating in a sequence of distinct switching states. Fig. 2 illustrates the gating signals over a single AC cycle, while Fig. 3 depicts the corresponding conduction paths of the switches and capacitors. Through controlled transitions between these states, the inverter alternately connects the DC source and switched-capacitor cell in parallel or series, enabling the generation of output levels. The following section provides a detailed explanation of each switching state and its role in achieving the five-level output.

Output +V: Fig. 3(a) illustrates the current flow path during the generation of the output voltage +V. In this stage, the switched capacitors C1 and C2 are connected in parallel and are charged directly from the source while simultaneously supplying the modulated +V voltage to the output. Since the capacitors are being recharged as they deliver power, no voltage decay occurs during this operation.

Output +2V: Fig. 3(b) illustrates the current flow path during the generation of the output voltage +2V. In this stage, the switched capacitors are connected in series to produce the +2V output. Because the operation alternates between the switching states shown in Fig. 3(a) and Fig. 3(b), the capacitor voltages remain balanced and stable despite not being able to charge at 3(b).

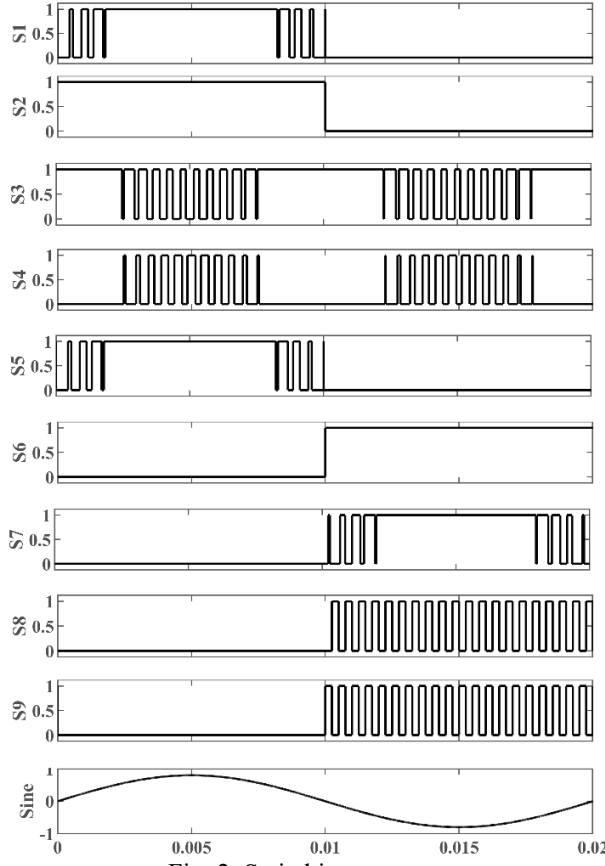


Fig. 2. Switching sequence

Output 0: Fig. 3(c) and Fig. 3(g) illustrate the zero-output state during the positive and negative operation cycles. In this state, the output is disconnected from both the input capacitors and the source, and the circuit operates in a freewheeling mode.

Output -V: Fig. 3(e) illustrates the negative voltage ($-V$) generation stage. In this mode, switches S6 and S7 are conducting, and the switched capacitors are in parallel mode to supply the negative output voltage $-V$. When the output voltage is zero or $-2V$, switch S8 conducts and charges capacitor C3 through diode D1. When the capacitors are configured in parallel mode, S8 turns off while S9 turns on, allowing the charge from C3 to be transferred to C1 and C2. This continuous charging process ensures that the capacitor voltages remain replenished and stable.

Output -2V: Fig. 3(f) illustrates the $-2V$ voltage generation process. In this stage, the switched-capacitor cell is configured in series, while switches S1 and S2 remain on. The circuit alternates between the operating states in Fig. 3(e) and Fig. 3(f) to maintain stable capacitor voltages.

Positive current absorption: Fig. 3(d) shows the reactive current absorption during the positive cycle. The capacitors are in a parallel configuration, and current flows through the diodes of switches S6 and S7.

Negative current absorption: Fig. 3(h) shows the reactive current absorption when the current is in a negative cycle. The switched capacitors are in a parallel configuration, and the diodes of switches S1 and S2 conduct.

Table I

SWITCHING TABLE FOR THE PROPOSED TOPOLOGY

	S1	S2	S3	S3'	S4	S5	S6	S7	S8	S9
+V	1	1	1	1	0	1	0	0	0	0
+2V	1	1	0	0	1	1	0	0	0	0
0 +ve	0	1	1	1	0	0	0	0	0	0
0 -ve	0	0	1	1	0	0	1	0	0	0
-V	0	0	1	1	0	0	1	1	0	1
-2V	0	0	0	0	1	0	1	1	1	0

Table I presents the switching sequence for the proposed topology. As shown, switches S3 and S3' share identical gating signals, while switches S1 and S5 also operate with the same switching pattern.

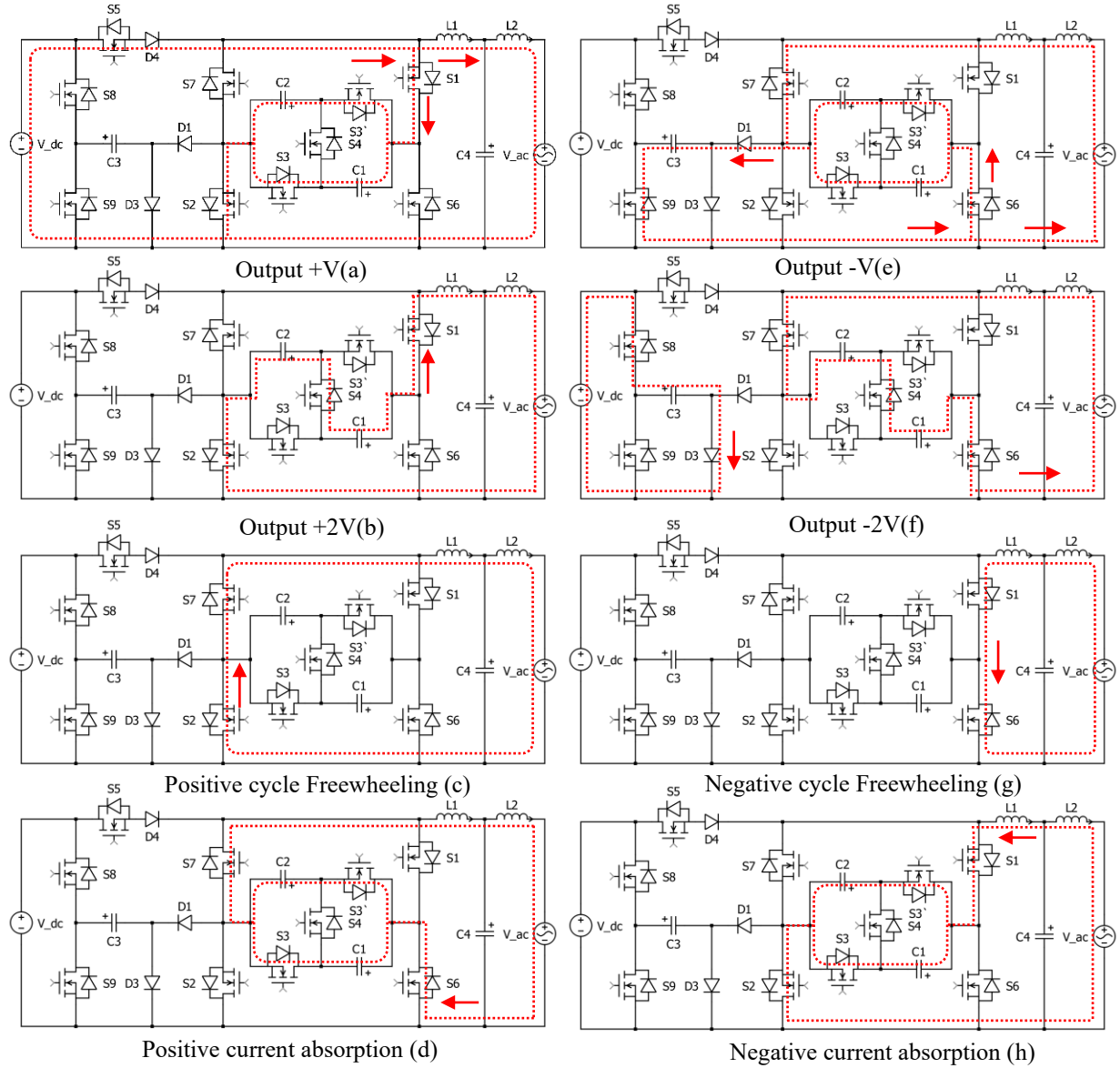


Fig. 3. Switching stages of the proposed inverter topology

III. EXPERIMENTAL SETUP AND CONTROL

A. Hardware-in-the-loop (HIL) setup

The HIL simulations were carried out on an OPAL-RT OP4520 real-time simulator. The inverter topology and control models were first developed in MATLAB/Simulink and deployed onto the OP4520 platform. A loop-back configuration was adopted, wherein the digital output ports of the simulator generated the PWM gating signals and were directly looped back into its digital input ports. Similarly, the analog output channels provided the simulated voltage and current signals, which were fed into the corresponding analog input channels. This arrangement ensured closed-loop testing and accurate emulation of controller feedback and gating actions. The OP4520 executed the simulations with a fixed time step of 20 μ s, as illustrated in Fig. 4.

In this setup, eight gate drivers were employed to control ten semiconductor devices. Among these, switches S2 and S6 operated at the fundamental grid frequency, while the remaining devices were modulated at 5 kHz. The complete set of simulation and electrical parameters used in the HIL evaluation is summarised in Table II.

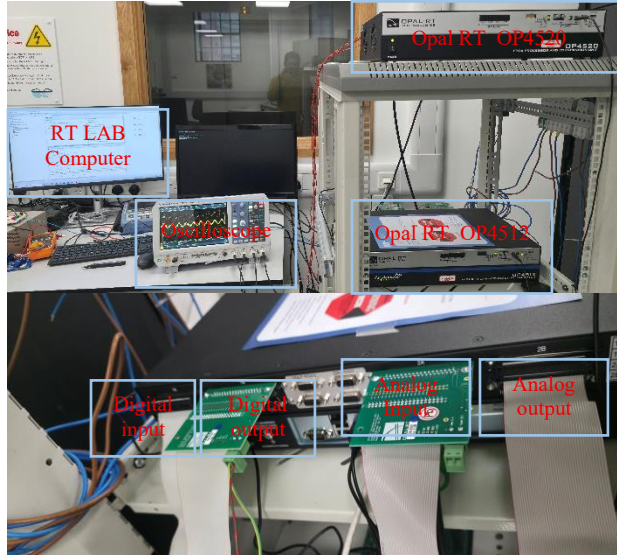


Fig. 4. HIL Setup

Table II
SPECIFICATIONS FOR THE EXPERIMENT

Parameters	Value
Filter size	10mH, 10mH, 8uF
Switching frequency	5kHz
Capacitor size	3*270uF
Input voltage	200V
Rated power	7kW
HIL simulator	Opal Rt
Sampling period	20 us

B. Developed Controller

Two separate controllers were implemented for the inverter to enable both standalone and grid-connected operation. In standalone mode, the inverter regulates its output voltage using a simple PI controller, with the measured voltage as the feedback and the duty cycle as the output, as shown in Fig. 5 (a). For grid-connected operation, a PI controller was employed in conjunction with Clarke and Park transformations. First, the sinusoidal voltage and current signals were transformed into a linearised form using Clarke and then Park transformations. These linearised values, together with the reference setpoints, were fed into the PI controller to generate the control signals. The outputs were then compensated, followed by the application of grid-voltage feedforward and cross-coupling feedforward terms. Finally, the inverse Park and Clarke transformations were applied to obtain sinusoidal control signals. The control diagram for grid-connected mode is shown in Fig. 5 (b).

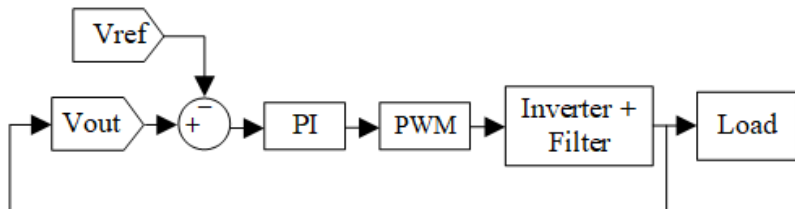


Fig. 5(a). Controller for off-grid mode operation.

The proposed topology was validated through HIL simulations under a wide range of operating scenarios. The performance evaluation considered several key metrics, including DC-link voltage stability, THD, efficiency, and the capability to regulate both active and reactive power. To further assess its robustness, the inverter was tested in various operating modes, including standalone operation, grid-connected operation, and the transition from standalone to grid-connected mode. The corresponding results demonstrate the ability of the proposed topology to maintain stable performance and reliable power quality across varying residential operating conditions.

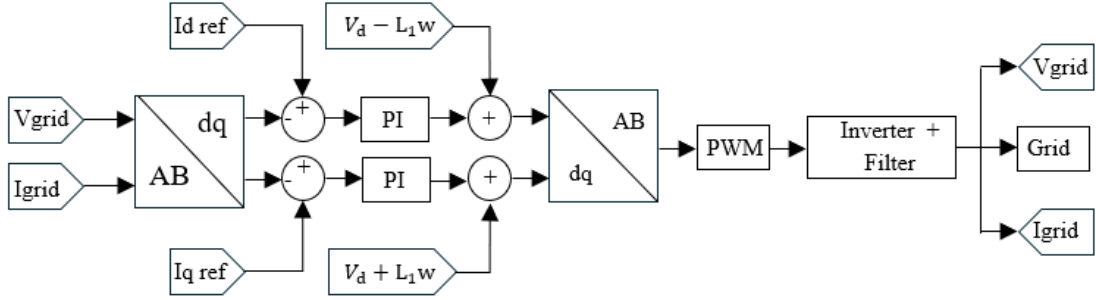


Fig. 5 (b). Grid-connected mode controller

IV. EXPERIMENTAL RESULTS AND DISCUSSION

A. Standalone operation

In standalone operation, the proposed inverter was configured to operate in voltage regulation mode with a reference output of 230 V (rms) at 50 Hz. The inverter's performance was evaluated under both steady-state and dynamic load conditions.

Fig. 6 presents the steady-state waveforms of the inverter, including the five-level unfiltered output voltage, the filtered sinusoidal voltage, and the corresponding load current. The unfiltered staircase waveform clearly demonstrates the five-level operation of the topology, while the filtered voltage exhibits a near-sinusoidal profile with a total harmonic distortion (THD) of 3.2%, well within the IEEE 519 harmonic limits for low-voltage residential applications. Under a load of 4.4 kW, the inverter achieved a peak efficiency of 96.35%, confirming the suitability of the proposed design for high-efficiency residential power conversion

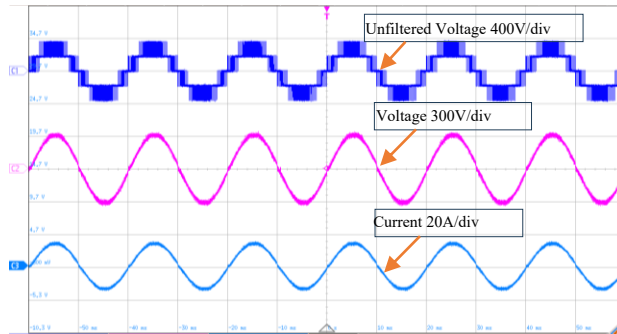


Fig. 6. Steady state waveforms

To further assess dynamic performance, the inverter was subjected to a step load change from 3.3 kW to 1.1 kW. The corresponding voltage and current responses are illustrated in Fig. 7. It is observed that the inverter maintains voltage regulation within $\pm 1\%$ of the reference value, with minimal overshoot and a rapid settling time. This demonstrates the ability of the proposed topology to sustain stable operation during abrupt load variations, which is essential for standalone residential systems with highly variable demand profiles.

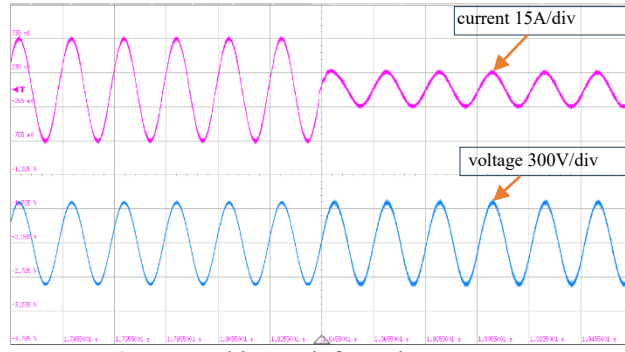


Fig. 7. get this graph from the OPAL-RT

B. Grid-connected operation

The inverter was tested under various conditions to verify its performance in grid-connected mode. The following sections discuss various test conditions and case studies performed.

a. Steady state and transient conditions

In grid-connected mode, the inverter was evaluated under steady-state and dynamic load conditions to validate its current regulation and power quality. Fig. 8 illustrates the steady-state waveforms, showing the grid voltage, inverter current, and the unfiltered five-level inverter voltage. The current is observed to be in phase with the grid voltage, confirming unity power factor operation. When the injected grid current was increased from 10 A to 15 A, the transition occurred smoothly, with negligible overshoot and a settling time within one grid cycle. The five-level staircase waveform demonstrates correct operation of the proposed topology, while the grid-injected current exhibited a near-sinusoidal profile with a THD of less than 3%, complying with IEEE 519 standards for residential grid interconnection.

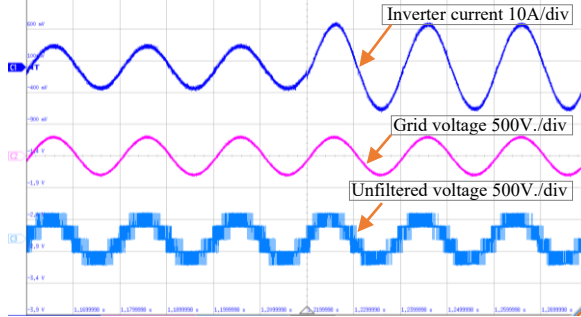


Fig. 8. Current, voltage & five-level voltage on dynamic conditions

The inverter was further tested in power factor correction (PFC) mode to verify its reactive power control capability. Fig. 9 presents the corresponding waveforms when the inverter injected 5 A and 15 A active current, along with 1.5 A and 4.5 A reactive current, respectively. A clear phase shift of approximately 16.7° (0.95 PF) between the grid voltage and injected current can be observed, demonstrating effective reactive power regulation. The transition between active and reactive power injection was achieved smoothly without oscillations or distortion, confirming the robustness of the proposed control strategy.

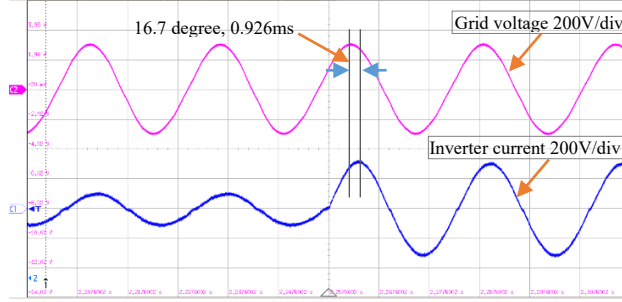


Fig. 9. Grid voltage and inverter current in power factor correction mode

These results establish that the proposed topology not only maintains stable operation at unity power factor but also provides flexible active and reactive power support, enabling compliance with modern grid codes that require residential inverters to contribute to grid stability under varying operating conditions.

b. Ride through capability

The ride-through capability of the proposed topology was evaluated in accordance with the EN 50549-1 standard, which specifies voltage sag and fault tolerance requirements for grid-connected inverters in Europe. According to this standard, the inverter must: (i) remain operational under a grid voltage reduction to 0.8 pu, (ii) ride through a 0.5 pu sag for at least 1 s, and (iii) withstand a short-duration dip to 0.2 pu for 150 ms.

Fig. 10 presents the experimental waveforms of the grid voltage, the five-level inverter output voltage, and the grid-injected current under these sag conditions. Under a 0.8 pu sag, the inverter continued injecting rated current into the grid with no observable distortion or loss of synchronisation, demonstrating stable operation. During the 0.5 pu sag, the inverter maintained continuous operation for 1 s while regulating the current smoothly, with THD measured below 5%. Finally, under the most severe condition of a 0.2 pu dip for 150 ms, the inverter successfully sustained current injection without tripping, and the current profile remained sinusoidal with minimal overshoot (<5%) upon recovery.

The zoomed-in waveforms further confirm that the proposed control strategy effectively regulates current even under depressed grid voltages, while the five-level output waveform preserves its stepped structure without collapse. These results validate that the proposed topology satisfies EN 50549-1 requirements. Importantly, the inverter's ability to maintain stable operation during sags enhances grid reliability and supports the integration of residential-scale renewable generation.

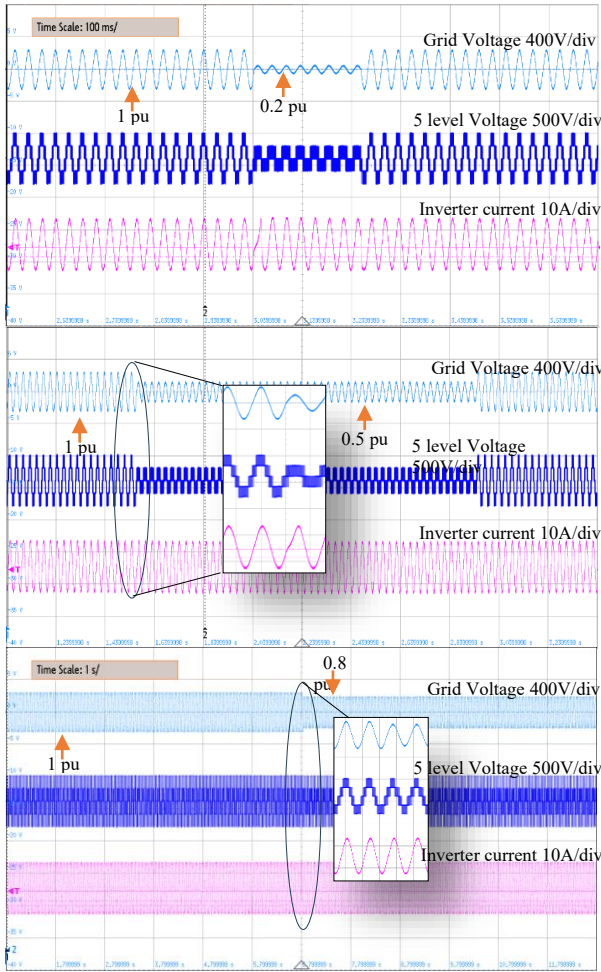


Fig. 10. Performance of the converter under grid voltage sag

c. Capacitor voltage balancing

Stable capacitor voltage regulation is essential for the reliable operation of multilevel and switched-capacitor topologies, particularly under conditions of reduced capacitance and high-power operation. To validate the robustness of the proposed inverter, the DC-link and switched-capacitor voltages were monitored under different load conditions. Fig. 11 illustrates the measured capacitor voltages when the inverter delivers 5 A and 15 A output currents at unity power factor. Capacitors C1 and C2 form the switched-capacitor cell, while C3 serves as the charge pump capacitor.

The measured results confirm that all capacitors maintain voltages around 200 V, with a maximum fluctuation of approximately ± 10 V (i.e., $\pm 5\%$ ripple). Even under higher load conditions, the capacitor voltages only drop to ~ 190 V, indicating strong voltage stability. Importantly, C1 and C2 remain well balanced throughout operation, as their voltages are equalised during the alternating series-parallel switching cycles. This demonstrates the inherent self-balancing property of the proposed topology, which eliminates the need for additional voltage-sensing or active balancing circuits.

Compared with conventional flying-capacitor multilevel inverters, where capacitor imbalance can accumulate over time and requires either bulky capacitance or complex control, the proposed configuration achieves stable operation with significantly smaller capacitor sizes. This directly reduces the overall DC-link capacitance requirement, improving power density and lowering cost while maintaining reliable performance under varying load conditions.

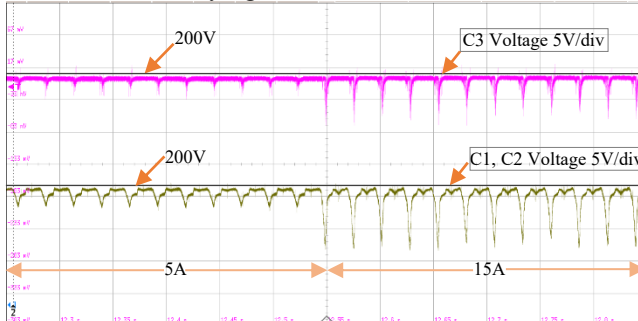


Fig. 11. Capacitor voltage during different load conditions

d. Voltage stress analysis

The voltage stress across the semiconductor devices was experimentally evaluated to validate the suitability of the proposed topology for practical implementation. Fig. 12 shows the measured switch voltages under steady-state operation, where each discrete step corresponds to approximately 200 V.

The results indicate that switch S5 experiences the highest stress, with peak values ranging from +200 V to -400 V (equivalent to 1.5 Vdc, where Vdc \approx 400 V). This elevated stress is attributed to its role in the charge-pump path, where it alternately blocks the full DC-link voltage in addition to the switched-capacitor voltage during certain states. In contrast, switches S1, S2, S6, and S7 sustain up to 400 V (\approx Vdc) stress, consistent with their role in forming the main H-bridge arms. The lowest stress levels, limited to approximately 200 V (\approx 0.5 Vdc), are observed across S3, S3', S4, S8, and S9, as these devices operate within the switched-capacitor cell where voltage sharing inherently limits their blocking requirement.

Compared with conventional multilevel inverters—where several devices routinely experience stress equal to the full DC-link voltage—the proposed configuration demonstrates a more favourable stress distribution. Specifically, only one switch (S5) sustains stress greater than Vdc, while the majority of devices are constrained to \leq Vdc, and several to just 0.5 Vdc. This distribution reduces the overall switching device voltage rating requirement and enables the use of lower-voltage MOSFETs with superior switching performance, improving efficiency and power density.

Thus, the voltage stress analysis validates that the proposed inverter topology maintains acceptable device stresses while leveraging its inherent series-parallel switching mechanism to minimise capacitor imbalance and reduce the need for uniformly high-voltage-rated devices.

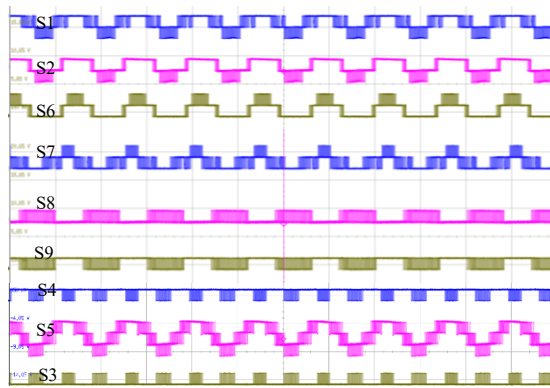


Fig. 12. Voltage stress analysis across the switches

e. Comparative analysis

A comparative study of the proposed topology with recently reported common-ground multilevel inverter configurations is presented in Table III. The comparison considers power rating, required DC-link capacitance, number of output levels, efficiency, and device count.

From the table, it is evident that the proposed topology achieves a 7 kW power rating with only $3 \times 270 \mu\text{F}$ capacitors, representing a ~70–85% reduction in DC-link capacitance compared to most existing designs that rely on $1000\text{--}2200 \mu\text{F}$ capacitors for similar or lower power ratings ([13], [15], [16], [17]). Even when compared to another high-power design in [9] (7 kW, $4 \times 270 \mu\text{F}$), the proposed configuration requires one capacitor less, while achieving slightly higher efficiency (96.4% vs. 96.1%) with the same five-level output and comparable switch count (10 vs. 9).

In terms of device requirements, the proposed inverter maintains a switch count similar to recent high-power topologies (10 devices), ensuring no increase in switching complexity. While the efficiency values across the compared designs range between 94.9% and 97.2%, the proposed configuration balances high efficiency, reduced capacitance, and higher power capacity, making it particularly suitable for residential and medium-scale PV applications.

Table III
COMPARISON OF DIFFERENT TOPOLOGIES

Paper	Rating	Capacitance	levels	Efficiency	Switches
[13]	500W	2*1000 uF	5	96.2 %	8
[14]	484W	3*1000 uF	9	96 %	9
[15]	600W	2*2200 uF	5	96.4 %	10
[16]	1000W	2*1000 uF	5	94.9 %	7
[17]	1000W	2*2200 uF	5	95 %	6
[20]	400W	3*1700 uF	9	97.2 %	10
[9]	7000W	4*270 uF	5	96.1%	9
Proposed	7000W	3*270 uF	5	96.4 %	10

Overall, the results in Table III demonstrate that the proposed inverter achieves a favourable trade-off between reduced capacitance, improved power capacity, and competitive efficiency, while retaining a practical switch count and output quality. This highlights the scalability and implementation feasibility of the proposed common-ground five-level topology compared with existing approaches.

V. CONCLUSION

A new five-level common-ground inverter topology has been proposed and validated for residential applications. By combining a switched-capacitor cell with a charge-pump mechanism, the topology ensures continuous capacitor charging throughout the AC cycle, thereby eliminating voltage decay at the negative peak and substantially reducing DC-link capacitance requirements. The design leverages the inherent self-balancing of the switched-capacitor network, obviating the need for active voltage regulation, and achieves stable operation across a wide range of loading conditions.

Extensive HIL simulations and experimental results confirm the effectiveness of the proposed design in standalone and grid-connected modes. The inverter demonstrated unity power factor operation, reliable reactive power control, and compliance with ride-through requirements under severe voltage sag conditions. Furthermore, it maintained capacitor voltage stability with only $\pm 5\%$ fluctuation and exhibited negligible leakage current due to the common-ground configuration. At a rated power of 7 kW, the inverter achieved 96.4% efficiency while reducing the capacitor size by over 70% compared with conventional CG topologies.

In summary, the proposed inverter provides a compelling combination of reduced capacitance, enhanced power density, high efficiency, and robust grid-support functionalities. These attributes make it a strong candidate for transformerless residential PV systems and establish a pathway toward compact, reliable, and grid-compliant next-generation inverter designs. Future work will focus on extending the concept with improved control, real hardware experiments and validating its long-term reliability under real-world operating conditions.

ACKNOWLEDGMENT

This work is part of the SuHSI (23/RDD/1034) project, and the authors in IERC thankfully acknowledge the support from the Sustainable Energy Authority of Ireland.

REFERENCES

- [1] R. Barzegarkhoo, M. Forouzesh, S. S. Lee, F. Blaabjerg, and Y. P. Siwakoti, ‘Switched-Capacitor Multilevel Inverters: A Comprehensive Review’, *IEEE Transactions on Power Electronics*, vol. 37, no. 9, pp. 11209–11243, Sep. 2022, doi: 10.1109/TPEL.2022.3164508.
- [2] Z. Huang, D. Zhou, L. Wang, Z. Shen, and Y. Li, ‘A Review of Single-Stage Multiport Inverters for Multisource Applications’, *IEEE Transactions on Power Electronics*, vol. 38, no. 5, pp. 6566–6584, May 2023, doi: 10.1109/TPEL.2023.3234358.
- [3] A. B. Barnawi, A. R. A. Alfifi, Z. M. S. Elbarbary, S. F. Alqahtani, and I. M. Shaik, ‘Review of multilevel inverter for high-power applications’, *Frontiers in Engineering and Built Environment*, vol. 4, no. 2, pp. 77–89, Jan. 2023, doi: 10.1108/FEBE-05-2023-0020.
- [4] D. Prasad and C. Dhananjayulu, ‘Reduced Voltage Stress Asymmetrical Multilevel Inverter With Optimal Components’, *IEEE Access*, vol. 10, pp. 53546–53559, 2022, doi: 10.1109/ACCESS.2022.3176110.
- [5] A. A. Estévez-Bén, A. Alvarez-Díazcomas, G. Macías-Bobadilla, and J. Rodríguez-Reséndiz, ‘Leakage Current Reduction in Single-Phase Grid-Connected Inverters—A Review’, *Applied Sciences*, vol. 10, no. 7, Art. no. 7, Jan. 2020, doi: 10.3390/app10072384.
- [6] X. Guo, X. Jia, Z. Lu, and J. M. Guerrero, ‘Single phase cascaded H5 inverter with leakage current elimination for transformerless photovoltaic system’, in *2016 IEEE Applied Power Electronics Conference and Exposition (APEC)*, Mar. 2016, pp. 398–401. doi: 10.1109/APEC.2016.7467903.
- [7] Md. M. Rahman, M. Shafayet Hossain, Md. S. Islam Talukder, and M. Nasir Uddin, ‘Transformerless Six-Switch (H6)-based Single-Phase Inverter for Grid-Connected Photovoltaic System With Reduced Leakage Current’, in *2020 IEEE Industry Applications Society Annual Meeting*, Oct. 2020, pp. 1–8. doi: 10.1109/IAS44978.2020.9334750.
- [8] R. Barzegarkhoo, S. S. Lee, S. A. Khan, Y. P. Siwakoti, and D. D.-C. Lu, ‘A Novel Generalized Common-Ground Switched-Capacitor Multilevel Inverter Suitable for Transformerless Grid-Connected Applications’, *IEEE Transactions on Power Electronics*, vol. 36, no. 9, pp. 10293–10306, Sep. 2021, doi: 10.1109/TPEL.2021.3067347.
- [9] A. Marahatta, S. Patra, H. Komurcugil, and S. Khadem, ‘Single Phase Five-Level Common-Ground Grid-Connected Inverter with Reduced DC link Capacitance’, in *2025 IEEE 19th International Conference on Compatibility, Power Electronics and Power Engineering (CPE-POWERENG)*, May 2025, pp. 1–6. doi: 10.1109/CPE-POWERENG63314.2025.11027303.
- [10] T. Roy, M. W. Tesfay, B. Nayak, and C. K. Panigrahi, ‘A 7-Level Switched Capacitor Multilevel Inverter With Reduced Switches and Voltage Stresses’, *IEEE Transactions on Circuits and Systems II: Express Briefs*, vol. 68, no. 12, pp. 3587–3591, Dec. 2021, doi: 10.1109/TCSII.2021.3078903.
- [11] J. F. Ardashir, M. Sabahi, S. H. Hosseini, F. Blaabjerg, E. Babaci, and G. B. Gharehpetian, ‘A Single-Phase Transformerless Inverter With Charge Pump Circuit Concept for Grid-Tied PV Applications’, *IEEE Transactions on Industrial Electronics*, vol. 64, no. 7, pp. 5403–5415, Jul. 2017, doi: 10.1109/TIE.2016.2645162.

- [12] M. N. H. Khan *et al.*, ‘A Common Grounded Type Dual-Mode Five-Level Transformerless Inverter for Photovoltaic Applications’, *IEEE Transactions on Industrial Electronics*, vol. 68, no. 10, pp. 9742–9754, Oct. 2021, doi: 10.1109/TIE.2020.3028810.
- [13] N. Sandeep, M. J. Sathik, U. R. Yaragatti, V. Krishnasamy, A. K. Verma, and H. R. Pota, ‘Common-Ground-Type Five-Level Transformerless Inverter Topology With Full DC-Bus Utilization’, *IEEE Transactions on Industry Applications*, vol. 56, no. 4, pp. 4071–4080, Jul. 2020, doi: 10.1109/TIA.2020.2996152.
- [14] S. S. Lee, Y. P. Siwakoti, R. Barzegarkhoo, and F. Blaabjerg, ‘A Novel Common-Ground-Type Nine-Level Dynamic Boost Inverter’, *IEEE Journal of Emerging and Selected Topics in Power Electronics*, vol. 10, no. 4, pp. 4435–4442, Aug. 2022, doi: 10.1109/JESTPE.2021.3104939.
- [15] J. S. Mohamed Ali, A. Hota, N. Sandeep, and D. J. Almakhles, ‘A Single-Stage Common Ground-Type Transformerless Five-Level Inverter Topology’, *IEEE Journal of Emerging and Selected Topics in Power Electronics*, vol. 10, no. 1, pp. 837–845, Feb. 2022, doi: 10.1109/JESTPE.2021.3095125.
- [16] S. S. Lee, Y. Yang, and Y. P. Siwakoti, ‘A Novel Single-Stage Five-Level Common-Ground-Boost-Type Active Neutral-Point-Clamped (5L-CGBT-ANPC) Inverter’, *IEEE Transactions on Power Electronics*, vol. 36, no. 6, pp. 6192–6196, Jun. 2021, doi: 10.1109/TPEL.2020.3037720.
- [17] S. Kumari, N. Sandeep, A. Verma, U. R. Yaragatti, and H. Pota, ‘Design and Implementation of Transformer-less Common-Ground Inverter With Reduced Components’, *IEEE Transactions on Industry Applications*, pp. 1–1, 2022, doi: 10.1109/TIA.2022.3165546.
- [18] Y. P. Siwakoti and F. Blaabjerg, ‘Common-Ground-Type Transformerless Inverters for Single-Phase Solar Photovoltaic Systems’, *IEEE Transactions on Industrial Electronics*, vol. 65, no. 3, pp. 2100–2111, Mar. 2018, doi: 10.1109/TIE.2017.2740821.
- [19] J. F. Ardashir, M. Ghassemi, B. Rozmeh, F. Blaabjerg, and S. Peyghami, ‘A Five-Level Transformer-Less Grid-Tied Inverter Structure With Capacitive Voltage Divider Concept With Leakage Current Elimination’, *IEEE Transactions on Industry Applications*, vol. 59, no. 5, pp. 6025–6036, Sep. 2023, doi: 10.1109/TIA.2023.3275928.
- [20] M. Jagabar Sathik, N. Sandeep, D. Almakhles, and F. Blaabjerg, ‘Cross Connected Compact Switched-Capacitor Multilevel Inverter (C3-SCMLI) Topology With Reduced Switch Count’, *IEEE Transactions on Circuits and Systems II: Express Briefs*, vol. 67, no. 12, pp. 3287–3291, Dec. 2020, doi: 10.1109/TCSII.2020.2988155.